PROTEINS: Structure, Function, and Genetics 42:383–389 (2001)

Modeling, Mutagenesis, and Structural Studies on the Fully Conserved Phosphate-Binding Loop (Loop 8) of Triosephosphate Isomerase: Toward a New Substrate Specificity

Brian V. Norledge,[1,2] Anne M. Lambeir,[3] Ruben A. Abagyan,[4] Antje Rottmann,[5] Anna M. Fernandez,[6] Vladimir V. Filimonov,[6] Martin G. Peter,[5] and Rik K. Wierenga[1,2]*

[1]*Biocenter Oulu and Department of Biochemistry, University of Oulu, Linnanmaa, Oulu, Finland*
[2]*European Molecular Biology Unit (EMBL), Heidelberg, Germany*
[3]*Laboratory of Medical Biochemistry, University of Antwerp (UIA), Wilrijk, Belgium*
[4]*Department of Molecular Biology, MB-37, Scripps Research Institute, La Jolla, California*
[5]*Institute for Organic Chemistry and Structure Analysis, University of Potsdam, Germany*
[6]*Department of Physical Chemistry, Faculty of Sciences, University of Granada, Granada, Spain*

ABSTRACT **Loop 8 (residues 232–242) in triosephosphate isomerase (TIM) is a highly conserved loop that forms a tight binding pocket for the phosphate moiety of the substrate. Its sequence includes the fully conserved, solvent-exposed Leu238. The tight phosphate-binding pocket explains the high substrate specificity of TIM being limited to the in vivo substrates dihydroxyacetone-phosphate and D-glyceraldehyde-3-phosphate. Here we use the monomeric variant of trypanosomal TIM for exploring the structural consequences of shortening this loop. The mutagenesis, guided by extensive modeling calculations and followed up by crystallographic characterization, is aimed at widening the phosphate-binding pocket and, consequently, changing the substrate specificity. Two new variants were characterized. The crystal structures of these variants indicate that in monomeric forms of TIM, the Leu238 side-chain is nicely buried in a hydrophobic cluster. Monomeric forms of wild-type dimeric TIM are known to exist transiently as folding intermediates; our structural analysis suggests that in this monomeric form, Leu238 of loop 8 also adopts this completely buried conformation, which explains its full conservation across the evolution. The much wider phosphate-binding pocket of the new variant allows for the development of a new TIM variant with a different substrate specificity. Proteins 2001; 42:383–389.** © 2000 Wiley-Liss, Inc.

Key words: triosephosphate isomerase (TIM); loop modeling; protein design; folding pathway; folding intermediate

INTRODUCTION

The triosephosphate isomerase (TIM) barrel $(\beta\alpha)_8$-fold provides a versatile scaffold on which various functions can be developed.[1,2] The eight central β-strands of the scaffold are labeled from the N terminus to the C terminus as B1–B8, respectively; the corresponding α-helices are labeled A1–A8. The βα-loops connecting β-strands B1–B8 to the subsequent α-helices A1–A8 are called loops 1–8, respectively. The active site of TIM barrel proteins is formed by these βα-loops. The first enzyme known to have the TIM-barrel fold was TIM. TIM is a dimeric glycolytic enzyme that interconverts dihydroxyacetone phosphate (DHAP) and D-glyceraldehyde-3-phosphate (GAP) during glycolysis (Fig. 1). The reaction mechanism of TIM has been extensively studied.[3] The residues directly involved in catalysis are Lys13, His95, and Glu167, found in loops 1, 4, and 6, respectively. In addition, residues from loops 6, 7, and 8 bind highly specifically to the phosphate moiety of the substrate.

Crystallographic studies have shown that loops 6 and 7 have an open conformation in the absence of active-site ligand and a closed conformation in the presence of ligand.[4,5] The tip of loop 6 moves approximately 7 Å on ligand binding, whereas for loop 7, the conformational switch concerns reorientation of two peptide planes. Loop 8 does not change conformation on ligand binding. Loops 6 and 7 are important for binding the ligand, as well as for catalysis. Mutagenesis studies on loop 6 have shown that shortening this loop results in large changes in the catalytic properties; in fact, the new variant becomes a methylglyoxal synthase.[6] Point-mutation studies on loops 6 and 7 pointed toward the importance of hydrogen-bonding interactions for stabilizing the closed conformation of these loops.[7,8] Loop 8 (residues 232–242) is not involved in catalysis; through interactions of the peptide NH groups of a 3_{10}-helical stretch, it binds the phosphate moiety of the ligand. A point-mutation study on loop 8 has rationalized the importance of Ser237 for the stability.[9]

Grant sponsor: European Union (EU); Grant number: BIO4-96-0670; Grant sponsor: Spain; Grant number: PB96-1446.

Vladimir V. Filimonov is on leave from the Institute of Protein Research of the Russian Academy of Sciences, Puschino, Russia.

*Correspondence to: Rik K. Wierenga, Department of Biochemistry, University of Oulu, Linnanmaa, FIN-90570, Oulu, Finland. E-mail: rik.wierenga@oulu.fi

Received 4 August 2000; Accepted 19 October 2000

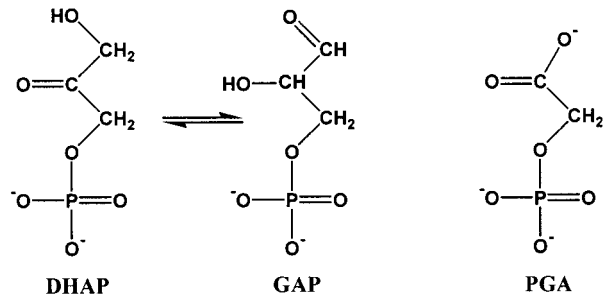

Fig. 1. Reaction catalyzed by TIM and the structure of the substrate analog PGA. PGA has a high affinity for wild-type TIM and its monomeric variants, for which K_i is equal to 26 and 73 μM, respectively.[12]

```
numbering                 232 234     238    242
                           |   |       |     |
secondary structure       β β           α α α α
wild type TIM             L V G G A S L K P E F
ml8TIM                    L V - S V - L K P E F
ml8bTIM                   L V G - - - L K P E F
secondary structure       β β           α α α
                           |   |       |     |
numbering                 232 234     238    242
```

Fig. 2. Sequences of loop 8 from wild-type trypanosomal TIM, ml8TIM, and ml8bTIM. The secondary structure of wild-type TIM is shown above the sequences, and the secondary structure of ml8bTIM is shown below. The anchor residues (in bold) were fixed in the modeling calculations. The sequence conservation of the LVGGASL stretch is very high. In fifty-four aligned TIM sequences, the following variations are observed: 232 (L54), 233 (V50,I4), 234 (G54), 235 (G48,K3,N1,S2), 236 (A54), 237 (S53,A1), and 238 (L53,W1). The stretch KPE forms the turn between the 3_{10}-helix and the helix A8; it can be of variable length. Position 242 (F52,L1,Y1) is also very highly conserved.

TIM has a very high substrate specificity. In fact, the only known substrates of TIM are DHAP and GAP. The active-site pocket extends from the catalytic residues at the bottom of the active-site pocket (His95 and Glu167) to the 3_{10}-helical stretch of loop 8, which binds the phosphate group. The tight phosphate-binding pocket limits the substrate specificity to DHAP and GAP. An examination of the phosphate-binding pocket reveals that loops 6, 7, and 8 (with loop 6 and loop 7 in the closed conformation) bind very tightly to the phosphate group of the active-site ligand. Of the six residues that make direct contact with the phosphate group, four are glycines (Gly173 from loop 6, Gly212 from loop 7, and Gly234 and Gly235 from loop 8). The peptide nitrogens of these residues and of Ser213 (loop 7) make hydrogen bonds with the phosphate oxygen atoms.

The high sequence conservation (Fig. 2) of some residues of loop 8 cannot be rationalized from the current data. Leu232 and Val233 are pointing inward into the hydrophobic interior close to the catalytic site. The glycines Gly234 and Gly235 are at the beginning of the 3_{10}-helical stretch, which binds the phosphate moiety. The presence of side-chains at these positions would interfere with phosphate binding. The side-chain of Ala236 is solvent-exposed and points to the adjacent loop 7, possibly explaining its high conservation. Ser237 is pointing inward and is stabilizing the 3_{10}-helix conformation of loop 8.[9] Leu238 is pointing outward, toward the adjacent loop 1, and its very high sequence conservation cannot be understood from the wild-type TIM structure. The very well conserved Phe242 is pointing inward into the same hydrophobic cluster as Val233.

Here we investigate the structural consequences of shortening loop 8. The mutagenesis of loop 8 is also aimed at widening the phosphate-binding pocket, thereby allowing for the creation of a TIM variant with a much broader substrate specificity.

MATERIALS AND METHODS

Loop Modeling

The modeling attempts were aimed at changing loop 8 to replace the tight phosphate-binding pocket with a wider binding pocket without disrupting the position of the catalytic residues Lys13, His95, and Glu167. For these studies, the monomeric variant ml1TIM of trypanosomal TIM[10] was used; its structure, complexed with the active-site ligand 2-phosphoglycollate (PGA; Fig. 1), is known. Loop 8 is anchored at its N terminus by Leu232 and Val233 and at its C terminus by Phe242, three buried hydrophobic residues forming part of framework secondary structure elements B8 and A8, respectively. By modifying the residues between Leu232 and Phe242 (Fig. 2), it seems possible to make alterations to this ligand-binding loop without disrupting the overall structure of the molecule. Loop modeling was carried out with the biased probability Monte Carlo (BPMC) facility of the ICM package[11] using protocols similar to those described previously.[10] All torsion angles for the residues between Leu232 and Phe242 were allowed to vary during the Monte Carlo simulations. Additionally, side-chain torsion angles of all residues containing atoms within 5 Å of loop 8 atoms were varied; this particularly concerns the side-chains of the adjacent loops, loops 1 and 7. A BPMC simulation of loop 8 minus Ser237 did indicate that the 3_{10}-helix would be disrupted, but no stable conformation was predicted. Further simulations with two residues (Ala236 and Ser237) removed predicted a clear conformation (8 kcal mol^{-1}) more favorable than the others. However, this version of loop 8 occupied the space of the phosphate-binding region; it also resulted in a large exposed area of three hydrophobic residues (Trp12, Leu21, and Leu24) that are normally buried by loop 8. Various alternative loop-8 sequences (always two residues shorter than the wild type) were tested in further BPMC calculations. Eventually, the ml8TIM sequence (Fig. 2) was predicted to have a stable conformation with a structure defining a wider phosphate-binding pocket.

ml8TIM was expressed and purified. No catalytic activity could be detected. The crystal structure of ml8TIM was determined (Table I) at a 3.2-Å resolution. The structure was refined without the refinement of individual *B* factors. The conformation of loop 8 could clearly be determined from the maps. The loop-8 structure differed from the predicted structure; for example, it protruded out into the wild-type phosphate-binding pocket (the purpose of widen-

TABLE I. Data Processing, Structure Solution, and Refinement Statistics for m18TIM

Data processing	
Resolution[a]	3.2 Å (3.4–3.2 Å)
R_{merge}[a]	11.5% (39.1%)
Completeness[a]	94.7% (95.2%)
$\langle I/\sigma \rangle$[a]	6.2 (3.2)
Number of reflections	4,027
B factor from Wilson plot	89 Å^2
Space group	$P6_3$
Cell dimensions (a, b, c)	92.3, 92.3, 53.1 Å
Cell dimensions (α, β, γ)	90.0° 90.0° 120.0°
Molecules per asymmetric unit	1
Molecular replacement	
Search Model	m11TIM
Rotation function, 1st peak	18.1 (5.3σ)
Rotation function, 2nd peak	13.7 (4.0σ)
Translation function (P6)	$C = 22.4\ R = 50.2$
Translation function ($P6_1$)	$C = 21.9\ R = 50.4$
Translation function ($P6_2$)	$C = 21.8\ R = 50.9$
Translation function ($P6_4$)	$C = 22.7\ R = 50.9$
Translation function ($P6_5$)	$C = 20.8\ R = 51.3$
Translation function ($P6_3$)	$C = 42.9\ R = 44.1$
Translation function, 2nd peak ($P6_3$)	$C = 14.9\ R = 52.7$
Refinement	
Protein atoms	1733
Water molecules	None
Other molecules	None
Overall *B* factor	80.0 Å^2
RMS bond-length deviation	0.026 Å
R factor	0.282
Free *R* factor (5% of the reflections)	0.394

[a]The numbers in parentheses refer to the highest resolution shell.

ing the pocket was, therefore, not achieved), and Leu238 of the new loop 8 was rotated inward into a cavity formed by the correlated movement of the Trp12 (loop 1) side-chain, which in turn was correlated with a large conformational change of loop 1. The movement of the Leu238 side-chain into this new hydrophobic cavity was not predicted, as main-chain angles of loop 1 were not varied in the modeling.

Further modeling and mutagenesis studies of loop 8 were carried out. Additional modifications to loop 8 with the conformation of loop 1 from ml8TIM were simulated. These calculations suggested that the even shorter loop-8 sequence of ml8bTIM (Fig. 2) (three residues shorter than the wild type) would adopt a stable conformation without any protrusion into the original phosphate-binding region. A favorable conformation was observed with a calculated free energy more than 3 kcal mol^{-1} lower than other conformations. This construct (ml8bTIM) was subsequently made and expressed, and the protein was also purified and characterized, including its full structural characterization.

Mutagenesis, Protein Expression, and Purification

Copies of an ml1TIM clone in a pET3a expression vector were already available,[10] and we used them as a template for site-directed mutagenesis of ml1TIM with the ExSite™ polymerase chain reaction (PCR)-based mutagenesis kit from Stratagene. Primers were obtained either from the EMBL primer synthesis service or from Applied Biotech. Ligated PCR products were used to transform competent XL1-Blue or DH5α competent *E. coli* cells that were plated onto LB-ampicillin agar. Successful clones were confirmed by direct sequencing with the PerkinElmer Big-Dye™ reaction kit and Abi Prism™ 310 genetic analyzer.

pET3a vectors containing the required mutants were used to transform competent BL21(DE3) *E. coli* cells. Cells were grown in a minimal (M9) medium at 18 or 25°C, and expression was induced in the mid-log phase with isopropyl-β-D-thiogalactopyranoside. Cells were lysed by being passed twice through a French press, and the proteins were purified as described previously.[12] The mass of the purified proteins was checked by mass spectrometry with a Reflex II matrix-assisted laser desorption/ionization time-of-flight mass spectrometer (Bruker–Daltonik, Bremen, Germany). For enzymatic studies, ml8TIM and ml8bTIM were separated from contaminant dimeric *E. coli* TIM by preparative gel filtration on Sephacryl S200HR (Amersham Pharmacia Biotech).

Protein Crystallization and Structure Determination

Crystallization conditions were screened with a sparse matrix screen[13] and were optimized as necessary with the protein dissolved in a 20 mM triethanolamine buffer (pH 8.0), 1 mM ethylenediaminetetraacetate (EDTA), 1 mM reduced dithiothreitol, 1 mM azide, and 100 mM NaCl. Crystals of ml8TIM grew in 1.0 M ammonium sulfate, 0.7 M lithium sulfate, and 0.1 M tris(hydroxymethyl)aminomethane (TRIS)/HCl (pH 8.0). ml8bTIM crystallized in a 0.1 M sodium citrate buffer (pH 5.5) with 20% polyethyleneglycol (PEG) 6000 and 5% tertiary butanol as the precipitants. X-ray data for ml8TIM and ml8bTIM were collected in house with an ENRAF–NONIUS rotating anode generator using a MAR345 image plate and also at the X11 beamline at the EMBL outstation at Deutsches Elektronen Synchrotron (DESY), Hamburg. The data were processed with the Denzo package[14] (Tables I and II). The structures were solved by molecular replacement with Amore[15] (Tables I and II). Refinement was carried out with the CCP4 suite of programs,[16] and manual rebuilding was done with the graphics program O.[17] The structures were refined to an *R* factor of 28.2% at a 3.2-Å resolution (ml8TIM) and 18.3% at a 2.65-Å resolution (ml8bTIM). The quality of the structures was assessed with PROCHECK.[18] Cavity analysis was done with the MSP package[19] with the same atomic radii as previously.[20] Protein Data Bank entries 1ml1 (liganded monomeric TIM, ml1TIM), 1mss (unliganded monomeric TIM, monoSS-TIM), and 5tim (wild-type TIM) were used for structural comparisons. ICM[11] was used to make Figures 4–6.

Solution Studies

Stability studies were done with differential scanning calorimetry (DSC) and the monitoring of circular dichroism (CD) spectra as a function of temperature. DSC was carried out with a VP-DSC microcalorimeter (MicroCal, United States) with a cell volume of 0.47 mL and a heating

TABLE II. Data Processing, Structure Solution, and Refinement Statistics for m18bTIM

Data processing	
Resolution[a]	2.65 Å (2.74–2.65 Å)
R_{merge}[a]	7.4% (18.1%)
Completeness[a]	92.9% (73.4%)
$\langle I/\sigma \rangle$[a]	8.7 (3.3)
Number of reflections	13,258
B factor from Wilson plot	40.0 Å^2
Space group	$P2_1$
Cell dimensions (a, b, c)	46.6, 88.5, 56.2 Å
Cell dimensions (α, β, γ)	90.0° 97.3° 90.0°
Molecules per asymmetric unit	2
Molecular replacement	
Search Model	m11TIM
Rotation function, 1st peak	28.5 (8.4σ)
Rotation function, 2nd peak	25.1 (7.4σ)
Rotation function, 3rd peak	14.3 (4.2σ)
Translation function, 1st peak (P2)	$C = 26.7\ R = 53.8$
Translation function, 2nd peak (P2)	$C = 25.8\ R = 54.7$
Translation function, both peaks (P2)	$C = 36.3\ R = 50.3$
Translation function, 1st peak ($P2_1$)	$C = 31.8\ R = 52.0$
Translation function, 2nd peak ($P2_1$)	$C = 33.0\ R = 52.0$
Translation function, both peaks ($P2_1$)	$C = 52.7\ R = 44.0$
Refinement	
Protein atoms	3587 (1807 + 1780)
Water molecules	145
Other molecules	2 (tertiary butanol)
Average *B*-factor main-chain molecule A[b]	35.5 Å^2 (2.2 Å^2)
Average *B*-factor side-chain molecule A[b]	39.1 Å^2 (2.8 Å^2)
Average *B*-factor main-chain molecule B[b]	35.2 Å^2 (2.2 Å^2)
Average *B*-factor side-chain molecule B[b]	35.2 Å^2 (3.0 Å^2)
Average solvent *B* factor	49.1 Å^2
RMS bond-length deviation	0.013 Å
R factor	0.183
Free *R* factor (5% of the reflections)	0.242

[a]The numbers in parentheses refer to the highest resolution shell.
[b]The RMS deviation in temperature factors for covalently bonded atoms is given in parentheses.

rate of 1.5 K/min. CD measurements were taken with a Jasco J-175 (Japan) instrument, with the sample heated from 278 to 348K in a 2-mm cell at a rate of 1 K/min. Protein concentrations of 50 and 6 μM were used in the DSC and CD measurements, respectively. The binding of the TIM substrate analog PGA (Fig. 1) was studied through the measurement of the effect (at a 1 mM concentration) on the temperature-induced unfolding in two buffers (10 mM TRIS, pH 7.6, 1 mM EDTA, and 25 mM sodium cacodylate, pH 7.0, 1 mM EDTA, 200 mM NaCl).

Enzymatic activity was determined at 25°C with GAP as a substrate as described[21] in a volume of 0.2 mL with a Spectramax340 microtiterplate reader (Molecular Devices, Sunnyvale, CA). To determine the kinetic parameters, the GAP concentration was varied between 1 and 22 mM, and the protein concentration was 1 mg/mL. Protein concentrations were determined with the method of Bradford.

RESULTS

Properties of ml8bTIM

ml8bTIM is a stable protein. The melting-temperature value, as determined by DSC and CD, is 58°C (Fig. 3),

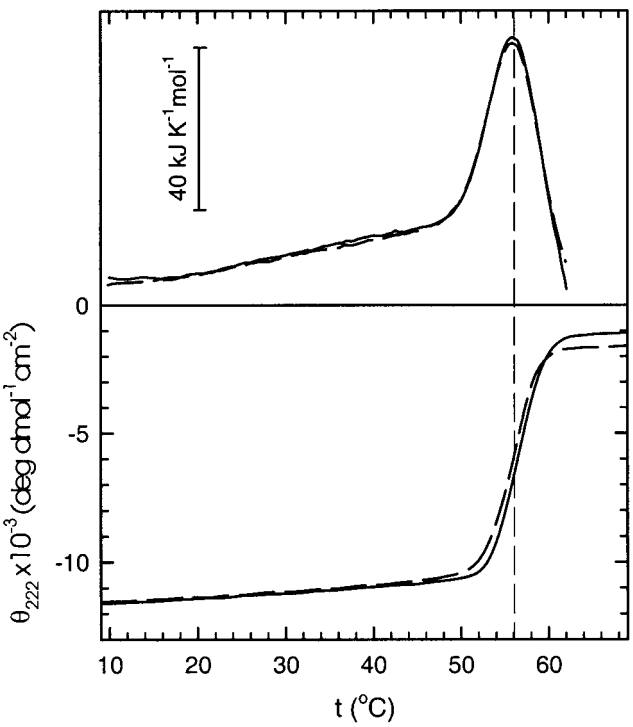

Fig. 3. Temperature dependency of the molar heat capacity, as measured by DSC (upper panel), and of θ_{222}, as measured by CD at 222 nm (lower panel) for ml8bTIM at pH 7.0, 200 mM NaCl, without ligand (solid lines), and in the presence of 1 mM PGA (dashed lines).

slightly higher than that seen for the reference molecule, ml1TIM.[10] The presence of PGA or NaCl had no significant effect on the melting-temperature value. With simple formulae, deduced elsewhere,[22] a lower limit of 4 mM can be placed on the K_d value for PGA. No catalytic activity was detected for ml8bTIM. The ml8bTIM crystals gave good diffraction, and details of the molecular replacement and refinement (to 2.65 Å) are given in Table II. The Ramachandran plot of ml8bTIM has no residues in disallowed regions. The two molecules of the ml8bTIM asymmetric unit superimpose with a root mean square (RMS) deviation in Cα positions of 0.22 Å. Loop 8 is well defined; it has relatively low B-factors and adopts the same conformation in both molecules.

Structure of Loop 1

In ml1TIM (and in dimeric wild-type TIM), Trp12 (in loop 1) is in a strained conformation (Chi1 = −73° and Chi2 = −7° in ml1TIM, and Chi1 = −72° and Chi2 = −19° in wild-type TIM). The modified loop 8 of ml8bTIM allows Trp12 to relax into a lower energy conformation (Chi1 = −179° and Chi2 = −113°) by swapping places with Leu238 (loop 8), as shown in Fig. 4. Consequently, the Leu238 side-chain is pointing into the core of the protein, forming part of a cluster of side-chains, including Val233 and Phe242 of loop 8; Ala10, Trp12, Leu21, Leu24, and Phe28 of loop 1; and Val41 of loop 2. The side-chains of loops 1 and 8 in ml8bTIM adopt unstrained conformations and are

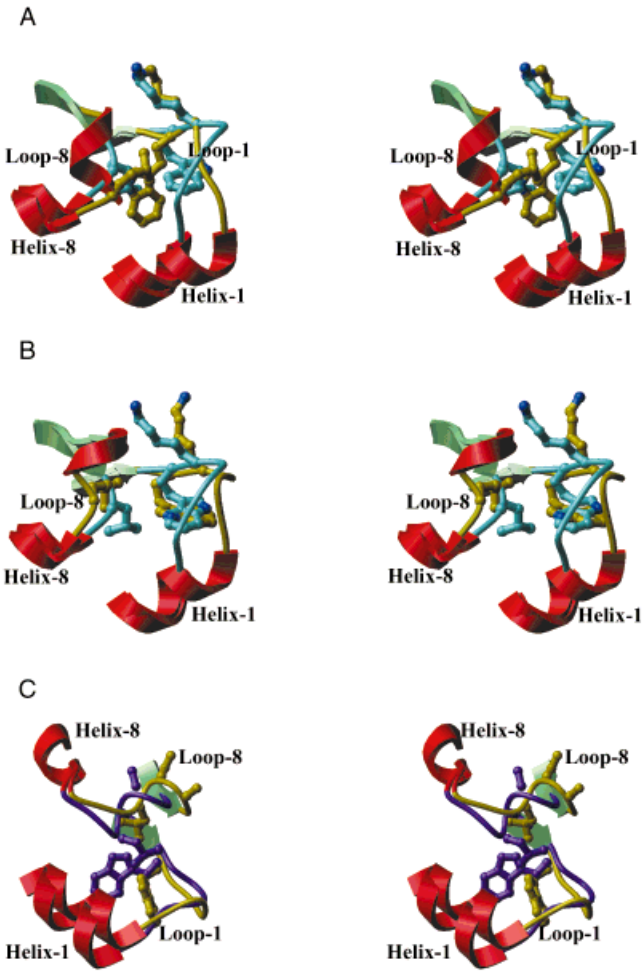

Fig. 4. Structure of loop 8. (A) Loops 1 and 8 of ml8bTIM (cyan) superimposed on those of ml1TIM (yellow). Leu238 is solvent-exposed in ml1TIM and is pointing inward in ml8bTIM; correlated with this movement are the rotation of the Trp12 side-chain, the different path of loop 1, and the unwinding of helix A1 by one turn in ml8bTIM. Also shown at the top of the figure is Lys13, which is in a similar conformation in both structures. (B) Loops 1 and 8 of ml8bTIM (cyan) superimposed on unliganded monoSS-TIM (yellow). Here, Trp12 occupies the same space in both structures, but in monoSS-TIM, helix A1 does not unwind, and Leu238 is not buried so deeply as in ml8bTIM. (C) Comparison of unliganded monoSS-TIM (yellow loop) and wild-type TIM (purple loop). The side-chains of Ala236, Ser237, and Leu238 are shown; because of the conformational switch from monoSS-TIM to wild-type TIM, Ser237 moves inward (it stabilizes the 3_{10}-helix of wild-type TIM), and Leu238 moves outward.

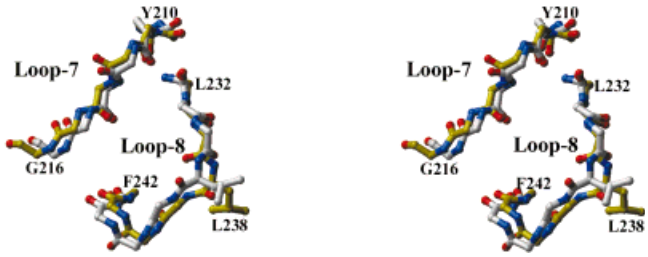

Fig. 5. Loops 7 and 8 of the ml8bTIM model (white) and the ml8bTIM X-ray structure (yellow). The loop-8 structure of the model is predicted by the loop modeling calculations in which the main-chain and side-chain torsion angles of the stretch 233–241 were modeled.

well packed, as only two small cavities are found in this region, both with a volume of 18 Å^3 (similar to ml1TIM, which also has two small cavities here, 24 and 19 Å^3). This places tight packing constraints on Leu238, turning it into a firm anchor for loop 8, an observation that correlates with the relatively low *B* factors for loop 8 and the slightly increased stability of ml8bTIM (Fig. 3). The conformational change of Leu238 is correlated with a large conformational change of loop 1, such that helix A1 begins one turn later in ml8bTIM (at Leu21) than in ml1TIM (where helix 1 begins at Pro18; Fig. 4). Loop 1 in ml8bTIM then moves up across the top of Leu238, burying Leu238 and exposing the ring nitrogen of Trp12. This movement does not, however, greatly affect the position or orientation of the catalytically important Lys13 (Fig. 4), the Cα atom of which has moved only 0.4 Å.

Interestingly, a similar switch of Leu238 and Trp12 was seen in the crystal structure of another unliganded monomeric TIM (monoSS-TIM[23]), although in this case helix A1 remains intact and loop 1 follows a path somewhat intermediate between the paths of ml1TIM and ml8bTIM (Fig. 4). The superpositioning of the unliganded monoSS-TIM structure on that of ml8bTIM (Fig. 4) shows that the planes of the tryptophan indole rings superimpose, but the rings are flipped with respect to each other.

Structure of Loop 8

The agreement between the predicted and X-ray structures of the ml8bTIM loop 8 is good everywhere apart from the conformation of Leu238 (Fig. 5). Two calculations can be made to compare the observed and predicted loop conformations: the atoms of the loops themselves can be superimposed (*loop superposition*), or the entire molecules can be superimposed (*framework superposition*). The RMS displacement from predicted positions of the 24 main-chain atoms of loop 8 is 1.4 Å in the framework superposition. In the loop superposition, the corresponding RMS difference is 1.0 Å. This good agreement between the predicted and observed structures of loop 8 is encouraging for loop-design protein engineering studies.[24–26] The largest difference is seen for Leu238, which is a result of the further small conformational changes to loop 1 in comparison with ml8TIM.

Structure of the Catalytic Site and New Binding Pocket

The conformation of loops 6 and 7 as seen in ml8bTIM is the same as in wild-type TIM (Fig. 6). The temperature factors of these loops are relatively high, as in wild-type TIM, suggesting that they have retained flexibility similar to that of their wild-type TIM counterparts. Most importantly, the crucial catalytic residues Lys13 (Fig. 4), His95, and Glu167 adopt the same conformation in ml8bTIM as they do in ml1TIM and wild-type TIM. Apparently, the catalytic machinery of TIM has been retained in ml8bTIM.

A clear picture of the new binding pocket can be obtained through a comparison of the surfaces of unliganded wild-

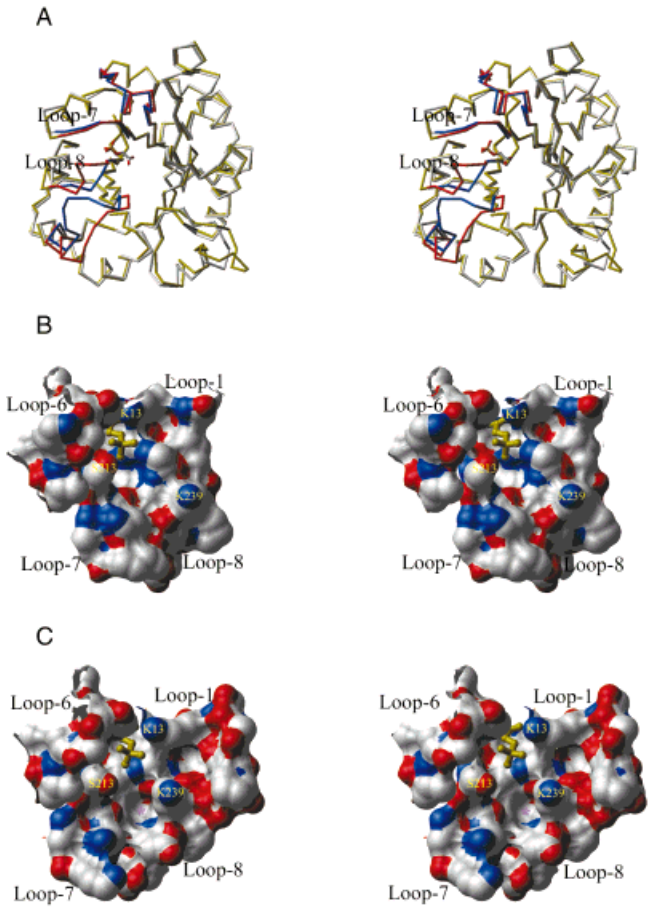

Fig. 6. New binding pocket. (A) The overall fold of ml8bTIM (yellow and blue Cα trace) superimposed on that of unliganded wild-type TIM (yellow and red Cα trace). The active site is identified by a PGA molecule from a superimposed liganded TIM structure. The blue and red loops indicate, counterclockwise from the top, loops 6, 7, 8, and 1. Loops 6 and 7 are similar in the two structures, whereas there are large differences for loops 8 and 1. (B) The molecular surface of the open form of wild-type TIM, with bound ligand (PGA) from a superimposed structure, showing loops 6, 7, 8, and 1. Carbon atoms are gray, oxygen atoms are red, and nitrogen atoms are blue. The view is similar to the view in A. (C) The corresponding surface of open ml8bTIM, again with PGA from a superimposed structure marking the catalytic site. The new binding pocket on the surface of the protein can clearly be seen (*) with a connecting groove between it and the catalytic site.

type TIM[27] and ml8bTIM (Fig. 6). The original phosphate-binding pocket, between Gly173 (loop 6), Ser213 (loop 7), and Gly234 (loop 8), has been widened, creating a connecting groove between the catalytic site and the deep new potential binding pocket between loops 7 and 8. This pocket is lined by main-chain atoms of Val214, Asn215 (loop 7), and Gly234 to Glu241 (loop 8); the hydrophobic bottom is shaped by the side-chains of Val214, Val233, Phe242, and Ile245 (Fig. 6).

DISCUSSION

Conserved Ala236-Ser237-Leu238 Sequence of Loop 8

In the structures of ml8bTIM and unliganded monoSS-TIM, the side-chains of Leu238 (loop 8) and Trp12 (loop 1) are swapped with respect to the conformation seen in wild-type TIM (Fig. 4). The conserved Leu238 (Fig. 2) is solvent-exposed in wild-type TIM. Trp12 is a buried residue, conserved in all TIM sequences, except in five, where it is replaced by a phenylalanine. The observation of the alternative, buried conformation of Leu238 in unliganded monoSS-TIM, ml8TIM, and ml8bTIM suggest that this conformational switch (Fig. 4) could have functional importance.

Furthermore, crystallographic binding studies with monoSS-TIM have shown that in the presence of active-site ligand, Leu238 switches back to the wild-type conformation, as seen from the comparison of the crystal structures of liganded and unliganded monoSS-TIM,[23] indicating that these conformations easily interconvert. In monoSS-TIM, the sequences of loops 1 and 8 are identical to those of wild-type TIM. The comparison of the structures of wild-type TIM and monoSS-TIM (unliganded) shows that the largest displacements occur for the Cα atoms of Ala236, Ser237, and Leu238 with displacements of 5.4, 5.7, and 3.8 Å respectively (Fig. 4).

Loops 1 and 8 are at the dimer interface in the wild-type TIM structure. In unliganded monoSS-TIM, Ser237 is solvent-exposed, and Leu238 is buried; as a result of the conformational switch, Ser237 becomes buried but well hydrogen-bonded,[9] and Leu238 becomes exposed. The ease of interconversion between the two states (as seen between liganded and unliganded monoSS-TIM) and the high sequence conservation of the Ala236-Ser237-Leu238 peptide suggest a functional role. Specifically, it suggests that the buried Leu238 conformation is essential for stabilizing the structure of the monomeric folding intermediate of wild-type TIM, which is known to exist transiently.[28–31] In this respect, the conformational heterogeneity of loop 1/loop 8 is very similar to the conformational heterogeneity seen for loop 4 in other structures of monomeric TIM:[23] two conformations of loop 4 are observed in structures of monomeric TIM. These structures also interconvert,[23] and one of them, as seen also in dimeric wild-type TIM, is stabilized (in wild-type TIM) by interactions across the dimer interface. Similarly, these monomer–monomer interactions across the wild-type dimer interface stabilize the wild-type loop 1/loop 8 conformation. Such structural plasticity is also seen in other examples of protein–protein interactions.[32,33] Apparently, the strained conformation of Trp12 and the bulk solvent position of the Leu238 side-chain in wild-type TIM are required to obtain an active-site pocket able to catalyze the TIM reaction with high efficiency.

Toward a New Substrate Specificity

The new active-site binding pocket of ml8bTIM is significantly larger and deeper than that of wild-type TIM (Fig. 6). An important lesson from these studies is that the widening of the phosphate-binding pocket could only be achieved when structural information from the first mutagenesis step (resulting in ml8TIM) was used because of the interactions between loops 1 and 8. The deep new pocket on the surface of the new protein is joined by a

connecting groove (near the original, wild-type TIM, phosphate-binding region) to the catalytic site. The open forms of loops 6 and 7 are unchanged in the new variant in comparison with the wild type (Fig. 6) and also have temperature factors similar to those of the wild type, suggesting that the opening–closing mechanism of these loops (both of which undergo conformational changes on ligand binding) are unchanged. This is particularly important for loop 6 because the closing of loop 6 includes a change in the orientation of the side-chain of Glu167, bringing it into its catalytic position.[5] The catalytic residues in ml8bTIM adopt the same positions as in unliganded monomeric and wild-type TIMs, indicating that the lack of catalytic activity of ml8bTIM is a result of a loss of binding rather than a loss of intrinsic catalytic capability. Modeling and experimental approaches for finding a suitable substrate for this new TIM variant have now been initiated.

ACKNOWLEDGMENTS

The authors thank the staff at EMBL (Hamburg) for their support during data collection at station X-11 and Dr. S. Haebel (Potsdam) for mass spectrometry measurements. A.M. Fernandez and V.V. Filimonov acknowledge a grant from Spain. The ml8bTIM structure was deposited at RCSB as 1DKW.

REFERENCES

1. Farber GK. An α/β-barrel full of evolutionary trouble. Curr Opin Struct Biol 1993;3:409–412.
2. Altamirano MM, Blackburn JM, Aguayo C, Fersht AR. Directed evolution of new catalytic activity using the alpha/beta-barrel scaffold. Nature 2000;403:617–622.
3. Knowles JR. Enzyme catalysis: not different, just better. Nature 1991;50:121–124.
4. Joseph D, Petsko GA, Karplus M. Anatomy of a conformational change: hinged "lid" motion of the triosephosphate isomerase loop. Science 1990;249:1425–1428.
5. Noble MEM, Zeelen JP, Wierenga RK. Structures of the "open" and "closed" state of trypanosomal triosephosphate isomerase, as observed in a new crystal form: implications for the reaction mechanism. Proteins 1993;16:311–326.
6. Pompliano DL, Peyman A, Knowles JR. Stabilisation o a reaction intermediate as a catalytic device: definition of the functional role of the flexible loop in triosephosphate isomerase. Biochemistry 1990;29:3186–3194.
7. Sampson NS, Knowles JR. Segmental movement: definition of the structural requirements for loop closure in catalysis by triosephosphate isomerase. Biochemistry 1992;31:8482–8487.
8. Sampson NS, Knowles JR. Segmental motion in catalysis: investigation of a hydrogen bond critical for loop closure in the reaction of triosephosphate isomerase. Biochemistry 1992;31:8488–8494.
9. Alvarez M, Zeelen JP, Mainfroid V, Rentier-Delrue F, Martial JA, Wyns L, Wierenga RK, Maes D. Triosephosphate isomerase (TIM) of the psychrophilic bacterium *Vibrio marinus*. Kinetic and structural properties. J Biol Chem 1998;273:2199–2206.
10. Thanki N, Zeelen JP, Mathieu M, Jaenicke R, Abagyan RA, Wierenga RK, Schliebs W. Protein engineering with monomeric triosephosphate isomerase (monoTIM): the modelling and structure verification of a seven-residue loop. Protein Eng 1997;10:159–67.
11. Abagyan R, Totrov M. Biased probability Monte Carlo conformational searches and electrostatics calculations for peptides and proteins. J Mol Biol 1994;235:983–1002.
12. Schliebs W, Thanki N, Eritja R, Wierenga RK. Active site properties of monomeric triosephosphate isomerase (monoTIM) as deduced from mutational and structural studies. Protein Sci 1996;5:229–239.
13. Zeelen JP, Hiltunen JK, Ceska TA, Wierenga RK. Crystallization experiments with 2-enoyl-CoA hydratase, using an automated 'fast-screening' crystallization protocol. Acta Crystallogr D Biol Crystallogr 1994;50:443–447.
14. Otwinowski Z. Oscillation data reduction program. In: Sawyer L, Isaacs N, Bailey S, editors. Proceedings of the CCP4 study weekend: "data collection and processing." England: Daresbury Laboratory; 1993. p 56–62.
15. Navaza J. AMoRe: an automated package for molecular replacement. Acta Crystallogr A 1994;50:157–163.
16. Collaborative computational project, no. 4. The CCP4 suite: programs for protein crystallography. Acta Crystallogr D Biol Crystallogr 1994;50:760–763.
17. Jones TA, Zou J-Y, Cowan SW, Kjeldgaard M. Improved methods for building protein models in electron density maps and the location of errors in these models. Acta Crystallogr A 1991;47:110–119.
18. Laskowski RA, MacArthur MW, Moss DS, Thornton JM. PROCHECK: a program to check the stereochemical quality of protein structures. J Appl Crystallogr 1993;26:283–291.
19. Connolly ML. Computation of molecular volume. J Am Chem Soc 1985;107:1118–1124.
20. Wierenga RK, Noble MEM, Davenport RC. Comparison of the refined crystal structures of liganded and unliganded chicken, yeast and trypanosomal triosephosphate isomerase. J Mol Biol 1992;224:1115–1126.
21. Lambeir AM, Opperdoes FR, Wierenga RK. Kinetic properties of triose-phosphate isomerase from *Trypanosoma brucei brucei*. A comparison with the rabbit muscle and yeast enzymes. Eur J Biochem 1987;168:69–74.
22. Shrake A, Ross PD. Ligand-induced biphasic protein denaturation. J Biol Chem 1990;265:5055–5059.
23. Borchert TV, Kishan KR, Zeelen JP, Schliebs W, Thanki N, Abagyan R, Jaenicke R, Wierenga RK. Three new structures of point mutation variants of monoTIM: conformational flexibility of loop-1, loop-4 and loop-8. Structure 1995;3:669–679.
24. Street AG, Mayo SL. Computational protein design. Struct Fold Des 1999;7:R105–109.
25. Regan L. Protein redesign. Curr Opin Struct Biol 1999;9:494–499.
26. Hellinga HW. Computational protein engineering. Nat Struct Biol 1998;5:525–527.
27. Wierenga RK, Noble MEM, Vriend G, Nauche S, Hol WGJ. Refined 1.83 Å structure of trypanosomal triosephosphate isomerase crystallized in the presence of 2.4 M ammonium sulphate. A comparison with the structure of the trypanosomal triosephosphate isomerase-glycerol-3-phosphate complex. J Mol Biol 1991;220:995–1015.
28. Lambeir AM, Backmann J, Ruiz-Sanz J, Filimonov V, Nielsen JE, Kursula I, Norledge BV, Wierenga RK. The ionization of a buried glutamic acid is thermodynamically linked to the stability of *Leishmania mexicana* triosephosphate isomerase. Eur J Biochem 2000;267:2516–2524.
29. Zabori S, Rudolph R, Jaenicke, R. Folding and association of triosephosphate isomerase from rabbit muscle. Z Naturforsch [C] 1980;35:999–1004.
30. Mainfroid V, Terpstra P, Beauregard M, Frère J-M, Mande SC, Hol WGJ, Martial JA, Goraj K. Three hTIM mutants that provide new insights on why TIM is a dimer. J Mol Biol 1996;257:441–456.
31. Rietveld AWM, Ferreira ST. Kinetics and energetics of subunit dissociation/unfolding of TIM: the importance of oligomerization for conformational persistence and chemical stability of proteins. Biochemistry 1998;37:933–937.
32. Sundberg EJ, Mariuzza RA. Luxury accommodations: the expanding role of structural plasticity in protein–protein interactions. Struct Fold Des 2000;8:R137–142.
33. Conte LL, Chothia C, Janin J. The atomic structures of protein–protein recognition sites. J Mol Biol 1999;285:2177–2198.